Extremophiles (2011) 15:379–389
DOI 10.1007/s00792-011-0366-3

ORIGINAL PAPER

Response to adverse conditions in two strains of the extremely halophilic species *Salinibacter ruber*

Jocelyn Brito-Echeverría · Marianna Lucio · Arantxa López-López · Josefa Antón · Philippe Schmitt-Kopplin · Ramón Rosselló-Móra

Received: 5 December 2010 / Accepted: 16 March 2011 / Published online: 3 April 2011

Abstract We have studied the response of the two closest relative strains M8 and M31 of *Salinibacter ruber* to environmental changes as the transition from exponential to stationary phase in a batch growth, and the submission to two different environmental stresses (dilution of the culture medium and temperature decrease). We monitored the changes in cultivability, ribosomal content by fluorescence in situ hybridization (FISH), and metabolic changes with high-field ion cyclotron Fourier transform mass spectrometry. In all cases, we could observe an important decrease in cultivability that was not accompanied by a decrease in FISH counts, pointing to a transition to viable but non-cultivable state rather than cell death. Furthermore, the metabolomic analyses indicated a common response of both strains to the different conditions assayed. Only a small portion of the detected masses could be annotated due to database constraints. Among them, the most remarkable changes could be attributed to modifications in the composition of the cell envelope, and especially in the cell membrane. We could track changes in the length or saturation of the fatty acids and in the composition of phospholipids involved in aminosugar, glycerolipid, and glycerophospholipid metabolic pathways.

Keywords Adverse conditions · Extremely halophilic bacteria · Metabolomics

Communicated by A. Oren.

Electronic supplementary material The online version of this article (doi:10.1007/s00792-011-0366-3) contains supplementary material, which is available to authorized users.

J. Brito-Echeverría (✉) · A. López-López · R. Rosselló-Móra
Marine Microbiology Group, Institut Mediterrani d' Estudis Avançats (CSIC-UIB), 07190 Esporles, Spain
e-mail: jocelyn.brito@uib.es

M. Lucio · P. Schmitt-Kopplin
Helmholtz Zentrum Muenchen, German Research Center for Environmental Health, Institute of Ecological Chemistry, Neuherberg, Germany

J. Antón
Departamento de Fisiología, Genética y Microbiología and Instituto Multidisciplinar de Estudios del Medio, Universidad de Alicante, Alicante, Spain

Introduction

High throughput analytical methods (genomics, transcriptomics, and proteomics) providing large sets of information have become important tools in metabolic engineering of producer cells, bioprocess analyses, and functional genomics (García et al. 2008; Schaub and Reuss 2008). Metabolomics, one of the latest "omic" technologies, allows the identification and quantification of intracellular and extracellular low molecular weight metabolites (<1 kDa) produced during bacterial growth (Mashego et al. 2007). The approach has proven to be sensitive enough to reveal environmental changes, such as small shifts in temperature, suggesting that metabolic profiling may be useful for investigating the functional response of microorganisms to environmental perturbations (Coucheney et al. 2008).

Microbial metabolomics has received much attention in recent years mainly because it supports and complements a wide range of microbial research. For example, the study of the structural and compositional changes occurring during the growth of bacterial populations (Ede et al. 2004; Fekete et al. 2010), the assessment of the metabolomic response of bacterial species to environmental variations (Coucheney et al. 2008), the study of the biogeographical patterns in the extremely halophilic bacterium *Salinibacter ruber* (Rosselló-Móra et al. 2008), or the metabolic adaptation of

bacterial species to the human gut (Samuel et al. 2007). The benefit of metabolome analyses is related to the fact that this kind of data enables direct access to the metabolic phenotype expressed under certain environmental conditions and, thus, together with metabolic fluxes, reflects the final outcome of cellular regulation processes at different levels, e.g., at transcriptional and/or translational levels (Schaub and Reuss 2008). The high-field ion cyclotron Fourier transform mass spectrometry (ICR-FT/MS) technique provides ultra highly resolved profiles of thousands of accurate mass values (*m/z*) that can be expressed as real elementary compositions. In addition, multivariate analysis permits the discriminative masses to be extracted for their further annotation into possible metabolites using bioinformatic tools such as the MassTRIX software (www.masstrix.org) (Suhre and Schmitt-Kopplin 2008). This program places the identified chemical compounds in KEGG (Kyoto *Encyclopedia of Genes and Genomes;* www.genome.jp/kegg/) (Kanehisa and Goto 2000) pathway maps taking into account the genomic context of the organism under study. The user can interpret the metabolic state of the organism in the context of its potential and, in the case of transcriptomic data, real enzymatic capacities (Suhre and Schmitt-Kopplin 2008).

The extremely halophilic bacterium *S. ruber* was first isolated from the salt saturated ponds of a Mediterranean solar saltern in Mallorca (Antón et al. 2002) and, since then, *S. ruber* representatives have been isolated from distinct hypersaline environments around the world (Antón et al. 2008). To reveal geographical differences in the metabolic pattern of the isolates we have recently used ICR-FT/MS (Rosselló-Móra et al. 2008). The approach allowed a non-targeted search for special metabolic traits considered to be relevant in the organism's phenotype and was shown to have higher resolution power than the molecular techniques previously applied in *S. ruber* population studies (Antón et al. 2008; Rosselló-Móra et al. 2008). In the present study, a combination of conventional cultivation methods and a metabolomic approach have been applied to the study of the main growth features of the closest *S. ruber* strains hitherto isolated (Peña et al. 2010). Special attention was paid to the changes occurring in the transition from exponential to stationary phase, and their response to two major different environmental stresses: dilution of culture medium, and decrease of the incubation temperature.

Materials and methods

Culture, growth curves, stress conditions, and metabolite extract preparation

M8 and M31 strains were grown in SW 25% (containing per litre: 195 g NaCl, 34.6 g $MgCl_2{\cdot}6H_2O$, 49.5 g $MgSO_4{\cdot}7H_2O$, 0.72 g $CaCl_2$, 5 g KCl, 0.17 g $NaHCO_3$, 0.65 g NaBr) emended with 0.2% yeast extract (pH 7.2) at 37°C with shaking (125 rpm). For each strain, growth curves were performed in duplicate for 14 days under identical incubation conditions. Optical density was measured daily. The number of cultivable cells was calculated on agar plates (SW 25%), total cell counts were microscopically measured with the fluorescent dye DAPI (4′-6-diamidino-2-phenylindole), and ribosome containing cells were detected by fluorescence in situ hybridization (FISH) using *S. ruber* probe EHB-412, as previously described (Antón et al. 1999, 2000). For the metabolomic analyses, cell pellets were collected daily by centrifugation of 2 mL of the cultures (16,000*g*, 2 min at 4°C). Pellets and cell-free supernatants were further processed for metabolite extractions (see below).

To study the metabolomic response of *S. ruber* to different stress conditions, both strains were grown under optimal conditions to reach the exponential phase (OD_{600} of 0.6–0.7). At this point, cultures were divided into three aliquots of 40 mL, one was kept as a control and the remaining two were submitted to the following stresses: in order to study the effect of the dilution of the medium, dilution stress was performed by adding 20 mL of sterile Milli-Q water to the same volume of culture, decreasing the salt content from 25% to 12.5% (w/v); and temperature stress was performed by incubating the culture at 4°C. The first two aliquots were incubated at 37°C. After 2, 16, and 40 h incubation under stress, subsamples were taken to quantify colony forming units (CFU) and DAPI (4′,6-diamidino-2-phenylindole stain) counts, and for metabolite extractions.

For metabolite extractions, 2 mL cell suspensions were centrifuged (16,000*g*, 2 min at 4°C). Supernatant was acidified by the addition of 100 µL of 98–100% formic acid and kept at −20°C until the chromatography separation, while pelleted biomass was suspended in 1 mL of Milli-Q water and sonicated to obtain a clear lysate extract. The lysate was also acidified by the addition of 50 µL of 98–100% formic acid. After the acidification, the clear lysate formed insoluble aggregates that could be separated from the soluble fraction by centrifugation (16,000*g*, 2 min at 4°C). The clear supernatant was stored for further fractionation, and the insoluble pellet was resuspended in 500 µL of methanol and stored at −20°C until use. Sample preparation resulted in three complementary fractions: the extracellular (E), cellular soluble (CS), and cellular insoluble fractions (CI). Both acidified extracellular and cellular soluble fractions were solid phase extracted using Bond Elut C18 columns (Varian Inc., Lake Forest, CA, USA). This chromatography enables the isolation of the organic molecules on the basis of their non-specific interaction and retention to the C18 material. This purification

removes the high-salt charge of the media and extracts, which may interfere during the electrospray procedure by ion suppression (Li et al. 2006). The retained fraction was recovered by the use of methanol (Rosselló-Móra et al. 2008).

ICR-FT/MS

Broad band mass spectra were acquired on a Bruker (Bremen, Germany) APEX Qe ICR-FT/MS with a 12T superconducting magnet and an Apollo I electrospray (ESI) source in negative and positive mode. The positive mode was selected as it showed the highest number of signals with the most annotated signals in the databases and also differentiated best in the multivariate statistics. The samples were infused in methanol with the microelectrospray source at a flow rate of 120 μL h^{-1} with a nebulizer gas pressure of 20 p.s.i and a drying gas pressure of 15 p.s.i. (200°C). Spectra were externally calibrated on clusters of arginine (10 mg L^{-1}in methanol), and calibration errors in the relevant mass range were always below 100 p.p.b., which is the prerequisite for an adequate elementary composition determination up to higher masses. Relative standard deviation in the intensity values of the peaks was routinely lower than 5% under our analysis conditions. The spectra were acquired with a time domain of 1 megaword (where 1 data word corresponds to 32 bits) and a mass range of 150–2,000 *m/z*. The spectra were zero filled to a processing size of 2 megawords. A sine apodization was performed before Fourier transformation of the time domain transient. The ion accumulation time in the ion source was set to 0.2 s and 1,024 scans were accumulated for one spectrum.

ICR-FT/MS spectra were exported to peak lists at a signal-to-noise ratio ($S/N = 1$) and they were aligned with an in-house software (Lucio et al. 2010) prior to further analysis. The possible elemental formulas were calculated for each peak in batch mode by a software tool written in-house (FORMULAE®). The generated formulas were validated by setting sensible chemical constraints (nitrogen rule, atomic oxygen to carbon ratio O/C $\leq$ (2 + C2), carbon C $\leq$ 100, oxygen 0 $\leq$ 80, nitrogen N $\leq$ 5, and sulphur S $\leq$ 1) (Hertkorn et al. 2007).

Different multivariate techniques from unsupervised principal component analysis (PCA) to supervised partial least square discriminative analysis (PLS-DA) were used in order to reduce the different datasets and extrapolate informative masses from the different experimental conditions. PCA is a mathematical procedure that uses an orthogonal transformation to convert a set of observations of possibly correlated variables into a set of values of uncorrelated variables called principal components. Partial least squares (PLS) projections to latent structures is a regression extension of PCA, which is used to find the relationship between a predictor matrix X and a response matrix Y, where the response matrix contains additional characterization of the samples in X, and in this contest are the classes. Besides, the PLS-DA and PLS modeling could be used to determine the relative concentration of the metabolites of interest. PLS-DA are the modeling often used in metabolomic field for classification of the samples (Barker and Rayens 2003; Bylesjö et al. 2006; Trygg and Wold 2002a, b). The difference in the phases was revealed also with PLS applying the orthogonal signal correction (OSC). The statistical analyses were carried out with SIMCA-P 11.5 (Umetrics, Umea, Sweden), and SAS version 9.1 (SAS Institute Inc., Cary, NC, USA). The masses with the highest regression coefficients were selected as discriminative for the different phases (Rosselló-Móra et al. 2008). These lists of masses were further reduced with the application of a Student's *t* test for paired samples, whose with significant differences were evaluated and assigned with the use of MassTRIX (Suhre and Schmitt-Kopplin 2008) and the Japanese (www.metabolome.jp) metabolome databases. In addition, MassTRIX gave valuable information through the identification of certain metabolites; in the meanwhile it was possible to characterize the experiments in relation with its biological context.

Results

Growth curve and stress cell dynamics

Both strains behaved differently in their OD changes, as shown in Fig. 1. The exponential phase of both organisms started 72 h after inoculation and occurred during 144–168 h, entering into the stationary phase at 216 h (M8

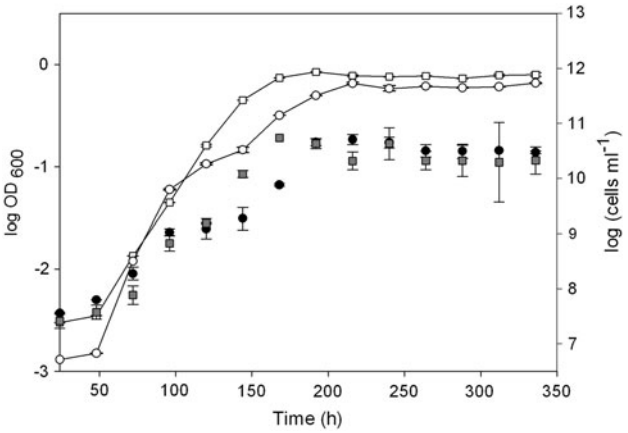

Fig. 1 Growth curves of *Salinibacter ruber* M8 (*squares*) and M31 (*circles*). Growth was monitored at OD_{600} (*empty symbols*) and by DAPI counts (*filled symbols*). Data are represented as log OD and log (cells mL^{-1}) with time. Plotted points are an average of two independent measurements

Table 1 Growth and cultivability of *S. ruber* cells during exponential and stationary phase. FISH counts were determined using specific probe EHB-412

Growth state	M8					M31				
	Time (hours)	Cells mL^{-1} ($\times 10^9$)[a]	CFU mL^{-1} ($\times 10^9$)[b]	% Cultivability	% FISH counts	Time (hours)	Cells mL^{-1} ($\times 10^9$)[a]	CFU mL^{-1} ($\times 10^9$)[b]	% Cultivability	% FISH counts
Exponential phase[c]	168	55	24	44	98	216	51	27	53	98
Stationary phase[d]	264 to 336	21	1.9	9	91	264 to 336	31	2.8	9	87

Standard deviation from 3.4 to 7.1 $\times$ 10^8 cells mL^{-1} (DAPI and FISH), and from 0.21 to 7.7 $\times$ 10^9 CFU mL^{-1}

[a] Determined by DAPI staining

[b] Determined by colony forming unit counts

[c] Maximum growth during the exponential phase

[d] Average of the last four points of the stationary phase

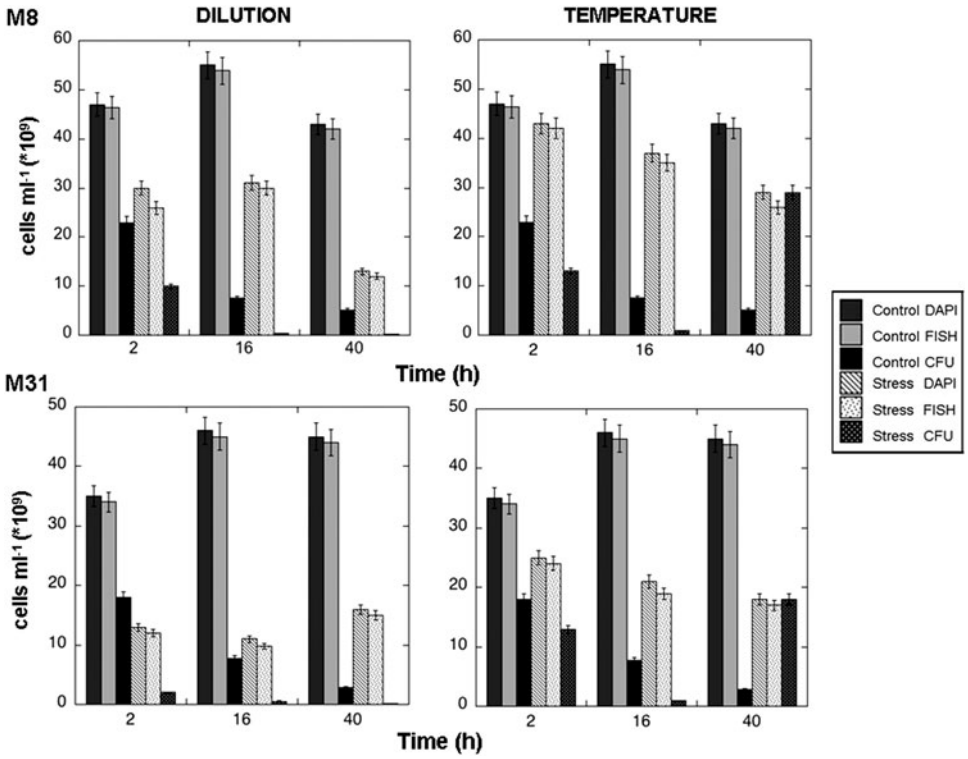

Fig. 2 Cultivability and cell counts of M8 and M31 strains under both stress conditions. All points correspond to the average of two independent measurements and represent the number of total cells determined by DAPI staining and FISH expressed as cells mL^{-1} with time, and the number of cells grown on agar plates expressed as CFU mL^{-1} with time

strain) and 240 h (M31 strain). Both cultures were inoculated with approximately the same amount of cells (10^9 cells mL^{-1}). However, the highest OD reached by M8 corresponded to 5.5 $\times$ 10^{10} cells mL^{-1}, as determined by DAPI counts, whereas the maximum value of M31 corresponded to 5 $\pm$ 0.05 $\times$ 10^{10} cells mL^{-1} (Fig. 1). In addition, during the exponential phase, both strains showed different generation times of 9.3 h for M8 and 10.1 h for M31. The lower OD reached by M31 but with higher cell counts can be explained by the formation of cell aggregates that biased the OD measures, a phenomenon that was not observed for M8 (data not shown). Cell numbers decreased in the stationary phase to 2.1 $\pm$ 0.19 $\times$ 10^{10} and 3.1 $\pm$ 0.04 $\times$ 10^{10} cells mL^{-1} for M8 and M31, respectively (Fig. 1). The cultivable fraction in the highest development of the exponential phase was equivalent to 44 and 53% of the corresponding DAPI counts in M8 and M31, respectively (Table 1). However, during the stationary phase, cultivability was reduced to 9% of the DAPI counts in both strains. FISH counts showed values that were close to 100% of the DAPI counts during the exponential phase, whereas the fraction decreased to about 87–91% in the stationary phase (Table 1).

As can be seen in Fig. 2, both strains responded similarly to the assayed stress conditions by reducing their total cell numbers and their cultivability. Both stresses promoted a continuous decrease of the total cell numbers observed by

DAPI, in some cases to nearly half of the initial value. These reductions in cell abundances were mirrored by the cultivable numbers, the latter showing more abrupt changes. Dilution promoted loss of cultivability in both strains (ranging from about 30 to <1%), whereas the fraction of FISH detectable cells did not decrease so strongly (in the worst case the detection rates dropped about 13%). However, the temperature effect showed a different dynamics. Both strains strongly reduced their cultivability to values from nearly 50% to about 2–4% of the DAPI counts but this cultivability depletion was recovered when the incubation time was prolonged for 40 h under low temperature (Fig. 2), at which point not only the initial rates were recovered but also increased to 100% of the DAPI counts.

Metabolome comparisons throughout the different phases of the growth curve

The complete set of metabolomes during the growth curve measurements rendered a total of 18,054 *m/z*, from which 7,174 could be attributed to known elementary compositions (Table S1). A multiple regression on the different phases revealed a clear separation among the growth states. PLS-DA models were applied to the three cellular fractions. In the three models created, variations between different growth states were observed (data not shown). Nevertheless, the extracellular fraction was revealed as the most descriptive (Fig. 3), since it was able to explain 96% of the variation of the data. The principal component analysis of this fraction showed a clear separation of the different phases,

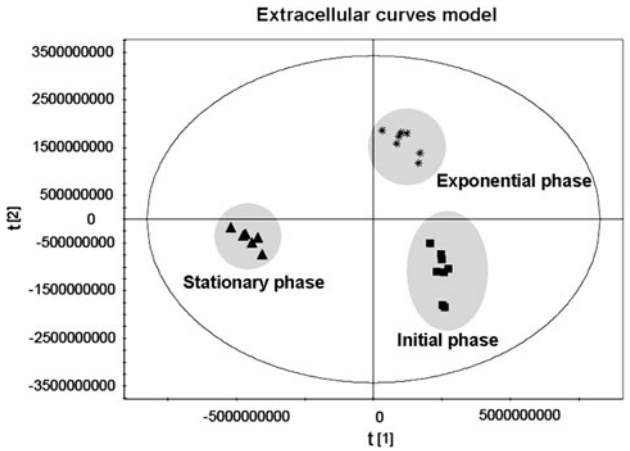

Fig. 3 PLS-DA model with all the extracellular fractions (E) analyzed in positive mode. The model explained 96% of the total variance and $Q^2(\text{cum}) = 0.95$. The predictive performance of the PLS model in relation to the three dependent variables (Y1 = initial phase, Y2 = exponential phase and Y3 = stationary phase) was always highly significant ($p < 0.001$ for all) showing three different groups corresponding to the initial, exponential and stationary growth phases. The model was validated with 200 permutations, revealing the absence of over fitting

revealing biological differences between the exponential and stationary phases (data not shown). To visualize the differences in their chemical composition, the masses associated with the highest loading values that were related to a specific elemental composition were represented in the van Krevelen projections (Fig. S1) (Holmes and Antti 2002; Wu et al. 2004). The most relevant markers for the common discriminative masses of the stationary phase metabolomes were mainly CHO and CHON compounds, with high (H:C) and low (O:C) ratios, indicating that these compounds were aliphatic in structure and associated with lipids (Fig. S1b).

The masses that revealed statistically significant differences between the exponential and stationary phases ($P < 0.05$) in the three analyzed fractions are shown in Table S1, and they were considered to reveal unique features for the different phases in both strains. The numbers of discriminative masses in each cellular fraction were between 800 and 990 where the common metabolome of both strains was formed by about 2,600 unique masses distinctly expressed in both growth phases. Finally we retrieved all the *m/z* values that showed intensities with increasing or decreasing values in both the stationary and exponential phases. In this regard, we observed during the stationary phase about 230 masses with increased intensities and 325 with decreased values. Those were the most discriminative for the assay and were used for the metabolite annotation (see below).

Metabolome comparisons in the different stresses assayed

PLS-DA models were created for each strain. In both cases, a clear difference between dilution and temperature stress conditions was observed (Fig. 4). From all the experiments conducted, the insoluble cellular fraction was chosen as representative in the PLS-DA model due to its goodness of fit in the prediction and in the explanation of the total variance. To reduce the impact of the over fitting (a test with 200 permutations was applied), for both models only one component was determined as significant [plot A: Q^2 (cum) = 0.3 $R^2(\text{Y}) = 0.5$, plot B: $Q^2(\text{cum}) = 0.8$ $R^2(\text{Y}) = 0.9$], expressing a valid and clear separation between both stress conditions assayed. This statistical evaluation allows differentiate and characterize the sample and gives a possible biological interpretation of data. The models built up with the extracellular and soluble cellular fractions also revealed a differentiation (data not shown) but the insoluble cellular fraction was chosen as the best model with more reliable differences between optimal (control) and stress conditions. In this sense and taking the highest values of the regression coefficients, two groups of discriminative masses characteristic for

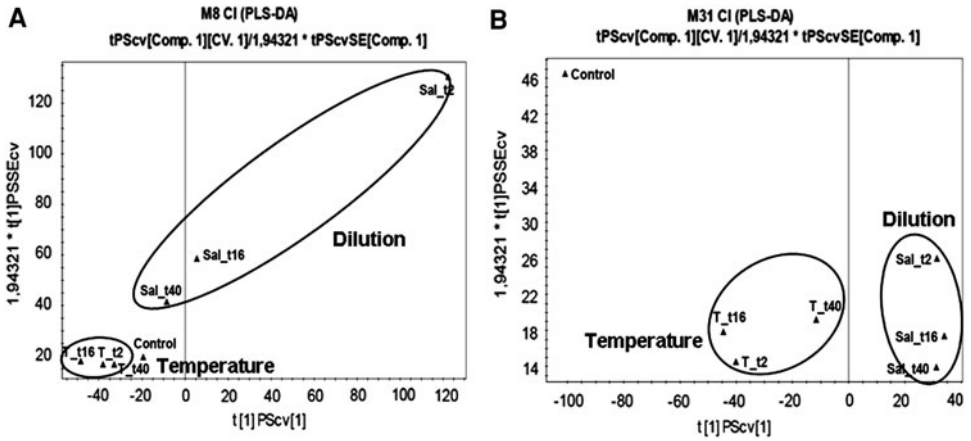

Fig. 4 The predicted scores (tPS) computed with seven cross validation rounds. In the PLS-DA model, the insoluble cellular fractions (CI) of the M8 **(a)** and M31 **(b)** strains analyzed in positive mode were included. The plot shows a good separation between both stress conditions. In particular, among the first component, the effect of dilution is negatively correlated with temperature, except in the M8 plot (**a**) in which the dilution effect at 2 h (Sal_t2) present a different behavior in relation to the rest of the diluted samples

each stress condition were isolated in both, M8 (Fig. 4a) and M31 (Fig. 4b) strains. Especially for M8 strain, we observed a remarkable difference during incubation time of dilution stress, in where the samples from 2 h showed a different behavior compared with the 16 and 40 h samples (Fig. 4a). Nevertheless, these observations are mainly due to differences in the intensity of characteristic masses expressed in each point rather than changes in their nature (data not shown).

The PCA analyses were conducted on the common metabolome of M8 and M31 only with the data obtained after 16 h stress due to the large size of the database generated with this set of samples. The initial total of 24,204 unique masses was reduced to 9,141 with the assignment of elementary compositions (CHONS elements, Table S2). As before, in addition to analyzing the PCA loading values, the intensity of the *m/z* values common in both strains was evaluated in order to recognize the masses that quantitatively varied its relative value (increased or decreased). The numbers of common unique masses with changing values in both stress conditions are summarized in Table S2. In almost all fractions, the number of masses with decreased intensities was higher than those increased.

Identification of masses and metabolic implications

The masses that were found to be discriminative in each of the different stress responses were crosschecked using the MassTRIX database and the annotation was done using the published genome of the M31 strain as a reference (Mongodin et al. 2005). For the transition to the stationary phase, only between 7 and 14% of the total discriminative masses could be annotated, and the majority of the masses remained unidentified. Of the annotated masses, approximately 12–50% (depending on the analyzed fraction) could be associated to the aminosugar, glycerolipid and glycerophospholipid metabolism pathways (Table 2). These results suggested that the most representative recognizable changes could be related to modifications on the composition of the cell envelope. As example, during exponential phase we could identify compounds involved in the synthesis of lipid A (*N*-Acetyl-D-glucosamine, *N*-Acetyl-D-mannosamine and *N*-Acetyl-D-galactosamine) that remained undetected during the stationary phase (Table 2). Moreover, during stationary phase we recognized changes in the saturation/unsaturation ratios and in the length of the acyl-chain of main membrane fatty acids, such as glycerolipids and glycerophospholipids (Table 2). For example, compounds with long acyl-chains and a high number of double bonds, such as 2-Acyl-sn-glycero-3-phosphoserine (R = C26:7), remained in low abundances during the stationary phase whereas, phospholipids with a low number of double bonds and shorter acyl-chains, such as 2-Acyl-sn-glycero-3-phosphoethanolamine (R = C19:3), were only detected in the stationary phase (Table 2).

The metabolome modifications occurring under the different stress conditions assayed rendered similar percentages of annotable metabolites. Again between 7 and 22% of the total stress discriminative masses (increased or decreased) could be identified and between 14 and 60% of them could be associated to glycerolipid, glycerophospholipid and fatty acid metabolisms, and biosynthesis of unsaturated fatty acid pathways (Tables 3, 4).

Both stress conditions produced a different transition of the fatty acid saturation/unsaturation ratios. During dilution stress, the phospholipids with a high number of double bonds decreased in intensity or remained undetected

Table 2 Proposed elemental composition of common masses increased or decreased during the stationary phase of *S. ruber* identified by the MassTRIX database

Detection in stationary phase	Cellular fraction	Exp. *m/z*	Proposed composition	Proposed name	Intensity of peak	Metabolic pathways involved
Decreased	E	302.06381	$C_8H_{16}NO_9P$	*N*-Acetyl-D-glucosamine 6-phosphate	UD	Aminosugar metabolism and phosphotransferase system (PTS)
Decreased	E	302.06381	$C_8H_{16}NO_9P$	*N*-Acetyl-D-mannosamine 6-phosphate	UD	Aminosugar metabolism
Decreased	E	302.06381	$C_8H_{16}NO_9P$	*N*-Acetyl-alpha-D-glucosamine 1-phosphate	UD	Aminosugar metabolism
Decreased	E	302.06381	$C_8H_{16}NO_9P$	*N*-Acetyl-D-galactosamine 6-phosphate	UD	Galactose metabolism and phosphotransferase system (PTS)
Decreased	E	429.07980	$C_{15}H_{21}NO_{10}P$	2-Acyl-sn-glycero-3-phosphoserine (R = C7:3)[a] (H+ replaced by Na+)	UD	Glycerophospholipid metabolism
Decreased	E	372.13888	$C_{15}H_{25}O_9$	sn-3-D-Galactosyl-sn-2-acylglycerol (R = C5:1) (H+ replaced by Na+)	UD	Glycerolipid metabolism
Decreased	CS	451.16083	$C_{18}H_{29}NO_{10}P$	2-Acyl-sn-glycero-3-phosphoserine (R = C10:2)	UD	Glycerophospholipid metabolism
Decreased	E	324.22921	$C_{19}H_{31}O_4$	1-Acylglycerol (R = C15:3)	UD	Glycerolipid metabolism
Decreased	E	400.25855	$C_{23}H_{37}O_4$	1-Acylglycerol (R = C19:4) (H+ replaced by Na+)	UD	Glycerolipid metabolism
Decreased	CS	687.31364	$C_{34}H_{51}NO_{10}P$	2-Acyl-sn-glycero-3-phosphoserine (R = C26:7) (H+ replaced by Na+)	UD	Glycerophospholipid metabolism
Increased	CS	332.10042	$C_{12}H_{22}O_7P$	1-Acyl-sn-glycerol 3-phosphate (R = C8:1) (H+ replaced by Na+)	ST	Glycerolipid and glycerophospholipid metabolism
Increased	E	368.10043	$C_{15}H_{22}O_7P$	1-Acyl-sn-glycerol 3-phosphate (R = C11:4) (H+ replaced by Na+)	ST	Glycerolipid and glycerophospholipid metabolism
Increased	CS	503.30018	$C_{25}H_{45}NO_7P$	2-Acyl-sn-glycero-3-phosphoethanolamine (R = C19:3)	ST	Glycerophospholipid metabolism

The intensity of masses and the metabolic pathways involved are also specified

UD under detection limit, *ST* detected in the stationary phase

[a] R = Cn:N; indicates the characteristics of acyl chains, where Cn is the number of carbons (length) comprising the chains and N the number of double bonds

(especially in the cellular soluble and insoluble fractions), while phospholipids with a low number of double bonds increased (Table 3). The opposite situation was observed for temperature stress where compounds with a high number of double bonds increased or were detected only under stress (e.g., 1-Acyl-sn-glycero-3-phosphocholine (R = C18:6)) and saturated compounds, such as 1-Acyl-sn-glycero-3-phosphocholine (R = C10:1), were reduced or remained undetected (Table 4).

In addition, a similar response was observed in the changes of the length of the acyl-chains of phospholipids under both stress conditions. For example, compounds with long acyl-chains (R = C26–C28), such as 2-Acyl-sn-glycero-3-phosphoserine (R = C28:3), decreased in intensity or remained undetected, whereas compounds with short acyl-chains (R = C10–C17) increased (Tables 3, 4). Exceptions to this rule were 1 and 2-Acyl-glycero-3-phosphocholine with short acyl-chains and low unsaturation (R = C10:1) that remained undetected during both stress conditions (Tables 3, 4).

Discussion

To understand whether the modifications of the environmental conditions were mirrored by a metabolic change of the cells, a metabolomic study was performed by means of high-resolution mass spectrometry (ICR-FT/MS), in a similar approach to that previously reported (Rosselló-Móra et al. 2008). We complemented the study by means of some physiological data as cultivability, total cell numbers, and FISH-detectable cells (as an indication of the ribosomal content). In all cases assayed, we observed a reduction of the cultivable fraction in comparison to the optimal growth during the exponential phase. During the stationary phase, only 9% of the DAPI stained cells grew onto plates, whereas the FISH counts remained about 90%. Similarly, in both stresses assayed, we observed a loss of cultivability. The prolonged stress conditions implied an abrupt drop of the cultivable fraction of both strains. Cultivability already reached the minimal values (<1%) after 16 h, but the cultures retained

Table 3 Proposed elemental composition of common masses increased or decreased under dilution stress conditions (16 h) and identified by the MassTRIX database

Detection	Cellular fraction	Exp. *m/z*	Proposed composition	Proposed name	Intensity of peak	Metabolic pathways involved
Decreased	CS	447.12901	$C_{18}H_{25}NO_{10}P$	2-Acyl-sn-glycero-3-phosphoserine (R = C10:4)[a]	UD	Glycerophospholipid metabolism
Decreased	CI	446.22852	$C_{19}H_{38}NO_7P$	1-Acyl-sn-glycero-3-phosphocholine (R = C10:1) (H+ replaced by Na+)	UD	Glycerophospholipid metabolism
Decreased	CI	446.22852	$C_{19}H_{38}NO_7P$	2-Acyl-sn-glycero-3-phosphocholine (R = C10:1) (H+ replaced by Na+)	UD	Glycerophospholipid metabolism
Decreased	CS	412.17283	$C_{20}H_{27}O_9$	sn-3-D-Galactosyl-sn-2-acylglycerol (R = C10:5)	UD	Glycerolipid metabolism
Decreased	CS	507.12640	$C_{21}H_{27}NO_{10}P$	2-Acyl-sn-glycero-3-phosphoserine (R = C13:6) (H+ replaced by Na+)	UD	Glycerophospholipid metabolism
Decreased	CS	537.17354	$C_{23}H_{33}NO_{10}P$	2-Acyl-sn-glycero-3-phosphoserine (R = C15:5) (H+ replaced by Na+)	UD	Glycerophospholipid metabolism
Decreased	CI	503.20478	$C_{24}H_{35}NO_7P$	2-Acyl-sn-glycero-3-phosphoethanolamine (R = C18:7) (H+ replaced by Na+)	UD	Glycerophospholipid metabolism
Decreased	CS	575.28344	$C_{25}H_{47}NO_{10}P$	2-Acyl-sn-glycero-3-phosphoserine (R = C17:0) (H+ replaced by Na+)	UD	Glycerophospholipid metabolism
Decreased	CS	502.21295	$C_{27}H_{34}O_7P$	1-Acyl-sn-glycerol 3-phosphate (R = C23:10)	UD	Glycerolipid and Glycerophospholipid metabolism
Decreased	CI	529.31653	$C_{27}H_{47}NO_7P$	2-Acyl-sn-glycero-3-phosphoethanolamine (R = C21:4)	UD	Glycerophospholipid metabolism
Decreased	CS	631.25137	$C_{30}H_{43}NO_{10}P$	2-Acyl-sn-glycero-3-phosphoserine (R = C22:7) (H+ replaced by Na+)	D (0.2)	Glycerophospholipid metabolism
Decreased	CS	596.38499	$C_{33}H_{56}O_7P$	1-Acyl-sn-glycerol 3-phosphate (R = C29:5)	UD	Glycerolipid and Glycerophospholipid metabolism
Decreased	CS	723.40814	$C_{36}H_{63}NO_{10}P$	2-Acyl-sn-glycero-3-phosphoserine (R = C28:3) (H+ replaced by Na+)	UD	Glycerophospholipid metabolism
Increased	E	451.16090	$C_{18}H_{29}NO_{10}P$	2-Acyl-sn-glycero-3-phosphoserine (R = C10:2)	I (1.4)	Glycerophospholipid metabolism

The intensity of masses and the metabolic pathways involved are also specified. Values in brackets represent the number of times

UD under detection limit, *I* increased value with respect to the control, *D* decreased value with respect to the control

[a] R = Cn:N; indicates the characteristics of acyl chains, where Cn is the number of carbons (length) comprising the chains and N the number of double bonds

similar FISH detection rates as the control state similarly to the exponential–stationary phase transition. However, it is remarkable that the prolonged incubation for 40 h at low temperature implied a 100% recovery of the cultivability. In this sense, this observation that did not correlate with the changes observed in their metabolome (see below).

In all cases, the qualitative metabolome composition of both strains in the same metabolic conditions was at least 95% identical and only <5% of the metabolites were unique in one or another strain. Isolating the common masses and focusing on those that were quantitatively characteristic (increased and/or decreased in their relative intensities), the degree of dissimilarity of the metabolomes was defined. The study was focused on the masses common to both strains but discriminative for the different conditions studied (i.e., those masses with modified intensities in comparison to the control conditions).

Among all conditions assayed and particularly in the proposed models (Figs. 3, 4), the metabolome composition under dilution and temperature stresses, and during the transition from the exponential to the stationary phase showed clear common metabolome shifts. Remarkable was the fact that the cells incubated at low temperature recovered the cultivability to 100% of the total cell numbers. This value doubled the rate observed during the optimal conditions of the exponential phase. Especially for this case, we analyzed the metabolomic composition after 40 h of temperature stress. Curiously, we did not find a valid model to evaluate possible differences between T16 and T40. The orthogonal PLS (OPLS and O2PLS) (Trygg and Wold 2002a, b) defined only a differentiation between the control state and both T16 and T40 (Fig. S2) incubations. Unfortunately, we could not identify the metabolites that may be related to the recovery of the cultivability, and a more detailed study with additional chemical analyses would be needed. A recovery of the culturable fraction is a phenomenon that has been observed in species such as *Vibrio parahaemolyticus*. In this case, a proportion of viable but non-culturable cells (VBNC) subjected to low temperatures remained viable after a temperature upshift, suggesting the re-growth of these cells rather than

Table 4 Proposed elemental composition of common masses increased or decreased under temperature stress conditions (16 h) and identified by the MassTRIX database

Detection	Cellular fraction	Exp. *m/z*	Proposed composition	Proposed name	Intensity of peak	Metabolic pathways involved
Decreased	CS	447.12901	$C_{18}H_{25}NO_{10}P$	2-Acyl-sn-glycero-3-phosphoserine (R = C10:4)[a]	UD	Glycerophospholipid metabolism
Decreased	CS	446.22842	$C_{19}H_{38}NO_7P$	1-Acyl-sn-glycero-3-phosphocholine (R = C10:1) (H+ replaced by Na +)	UD	Glycerophospholipid metabolism
Decreased	CI	446.22842	$C_{19}H_{38}NO_7P$	2-Acyl-sn-glycero-3-phosphocholine (R = C10:1) (H+ replaced by Na+)	UD	Glycerophospholipid metabolism
Decreased	CS	507.12640	$C_{21}H_{27}NO_{10}P$	2-Acyl-sn-glycero-3-phosphoserine (R = C13:6) (H+ replaced by Na+)	UD	Glycerophospholipid metabolism
Decreased	CI	503.20478	$C_{24}H_{35}NO_7P$	2-Acyl-sn-glycero-3-phosphoethanolamine (R = C18:7) (H+ replaced by Na+)	UD	Glycerophospholipid metabolism
Decreased	CI	554.33586	$C_{28}H_{52}O_7P$	1-Acyl-sn-glycerol 3-phosphate (R = C24:2) (H+ replaced by Na+)	UD	Glycerolipid and Glycerophospholipid metabolism
Decreased	CI	554.33586	$C_{30}H_{50}O_7P$	1-Acyl-sn-glycerol 3-phosphate (R = C26:5)	UD	Glycerolipid and Glycerophospholipid metabolism
Decreased	CS	723.40814	$C_{36}H_{63}NO_{10}P$	2-Acyl-sn-glycero-3-phosphoserine (R = C28:3) (H+ replaced by Na+)	UD	Glycerophospholipid metabolism
Increased	CI	216.13584	$C_{11}H_{19}O_4$	1-Acylglycerol (R = C7:1)	I (3)	Glycerolipid metabolism
Increased	CI	358.11682	$C_{16}H_{22}O_7P$	1-Acyl-sn-glycerol 3-phosphate (R = C12:5)	I (3)	Glycerolipid and Glycerophospholipid metabolism
Increased	CS	296.19782	$C_{17}H_{27}O_4$	1-Acylglycerol (R = C13:3)	S	Glycerolipid metabolism
Increased	CI	425.15708	$C_{18}H_{29}NO_7P$	2-Acyl-sn-glycero-phosphoethanolamine (R = C12:4) (H+ replaced by Na+)	S	Glycerophospholipid metabolism
Increased	CI	443.20501	$C_{19}H_{35}NO_7P$	2-Acyl-sn-glycero-phosphoethanolamine (R = C13:2) (H+ replaced by Na+)	I (3)	Glycerophospholipid metabolism
Increased	CS	497.14391	$C_{22}H_{27}NO_{10}P$	2-Acyl-sn-glycero-3-phosphoserine (R = C14:7)	I (1.5)	Glycerophospholipid metabolism
Increased	CS	450.27458	$C_{22}H_{42}O_7P$	1-Acyl-sn-glycero-3-phosphate (R = C18:1)	S	Glycerolipid and Glycerophospholipid metabolism
Increased	CS	450.27458	$C_{27}H_{39}O_4$	1-Acylglycerol (R = C23:7) (H+ replaced by Na+)	S	Glycerolipid metabolism
Increased	CS	504.30932	$C_{25}H_{46}NO_7P$	1-Acyl-sn-glycero-3-phosphocholine (R = C16:3)	S	Glycerophospholipid metabolism
Increased	CS	504.30932	$C_{25}H_{46}NO_7P$	2-Acyl-sn-glycero-3-phosphocholine (R = C16:3)	S	Glycerophospholipid metabolism
Increased	CI	575.28348	$C_{25}H_{47}NO_{10}P$	2-Acyl-sn-glycero-3-phosphoserine (R = C17:0) (H+ replaced by Na+)	I (3)	Glycerophospholipid metabolism
Increased	CS	526.29135	$C_{27}H_{44}NO_7P$	1-Acyl-sn-glycero-3-phosphocholine (R = C18:6)	S	Glycerophospholipid metabolism
				2-Acyl-sn-glycero-3-phosphocholine (R = C18:6)	S	Glycerophospholipid metabolism

The intensity of masses and the metabolic pathways involved are also specified. Values in brackets represent the number of times

UD under detection limit, *S* detected under stress condition, *I* increased value with respect to the control

[a] R = Cn:N; indicates the characteristics of acyl chains, where Cn is the number of carbons (length) comprising the chains and N the number of double bonds

resuscitation of all bacteria in the initial inoculum (Coutard et al. 2007). These changes might be a survival strategy for certain bacterial species. In our study, this phenomenon was observed even when the time of incubation at low temperature was prolonged up to 30 days (data not shown). The results suggested that, under low temperature incubation, *S. ruber* may generate a survival strategy to re-adapt to the new environmental conditions. This would promote a readjustment of their cellular machinery to shift the non-cultivable to a cultivable state.

Using the KEGG database through the MassTRIX search engine, we could only indentify between 7 and 22% of all the metabolome masses due to database constraints, while the most of the masses remained unannotated. We are aware that unannotated masses may be relevant for the understanding of the cellular changes occurred. However, we focused our work on the annotable masses that could explain the biological response to our experiments.

We could observe a depletion of masses associated with aminosugar metabolism (as LPS) during the stationary phase, and also a modification in the composition of phospholipids and fatty acids in their side chain length or saturation state. In dilution stress, the level of unsaturated

phospholipids decreased in intensity, while saturated phospholipids increased. On the other hand, the downshift of the incubation temperature promoted an increase in the unsaturated proportions of the phospholipids accompanied by a reduction in the length of their side chains. Previous reports of *S. ruber* have shown that polar lipids represented about 80% of the total lipid extract, and that changes in salinity from 25 to 19% and from 25 to 32%, did not produce significant differences in the lipid profile or in the saturation/unsaturation ratio of lipid fatty acyl-chains (Lattanzio et al. 2009). However, in our case we observed remarkable modifications due to a more abrupt change in the total content of salts (from 25 to 12.5%). At this point, we have to take into account that *S. ruber* grows optimally at total salt concentrations of 15–30%, requiring at least 15% for growth (Antón et al. 2002). A similar tendency has been reported in *Shewanella gelidimarina*, where the proportion of monounsaturated fatty acids was also regulated during hyper- and hypoosmotic stress, showing that the lipid packing and adaptational fatty acid composition responses were clearly influenced by salinity (Nichols et al. 2000). Also, a temperature downshift that would lead to solidification and impairment of membrane function could be counteracted by shortening of the chain length, thereby increasing the amounts of unsaturated fatty acids as signs of adaptation, as also observed in *Campylobacter coli* SP10 (Höller et al. 1998).

Using ICR-FT/MS, we have been able to visualize in a high dynamic range and with precision, thousands of relevant metabolites out of the immense chemical diversity that was dynamically changing during the stress situations. However, accurate metabolite identification and differentiation at the isomer level can only be undertaken using classical analytical chemistry approaches. Unfortunately, an important portion of the masses observed remained unannotated, and their identification would be relevant to understand additional changes occurring during the different metabolic situations experienced. Nevertheless, among the identifiable molecule changes, we observed that the modifications in the balance of molecules involved in the cell membrane components, which maintain an optimal fluidity and viscosity of the membrane, were more important than those occurring intracellularly. Environmental changes may have diverse effects on the function of membrane-associated enzymes including those required for the synthesis of envelope components, such as lipid A and peptidoglycan (DiRusso et al. 1999). We demonstrated that the pathways related to the synthesis and metabolism of cell envelope compounds in *S. ruber* could be the first line of defense guarding the organism from environmental stresses and trigger signals that lead to induction of cell growth or entry into quiescence (Denich et al. 2003; DiRusso et al. 1999).

Acknowledgments This work was supported by the projects CLG2009_12651-C02-01 and 02; and CE-CSD2007-0005 of the Spanish Ministry of Science and Innovation, and all three projects were also co-financed with FEDER support from the European Union. J. Brito-Echeverría was financed by the Government of the Balearic Islands, Ministry of Economy and Finance.

References

Antón J, Llobet-Brossa E, Rodríguez-Valera F, Amann R (1999) Fluorescence in situ hybridization analysis of the prokaryotic community inhabiting crystallizer ponds. Environ Microbiol 1:517–523

Antón J, Rosselló-Móra R, Rodríguez-Valera F, Amann R (2000) Extremely halophilic bacteria in crystallizer ponds from solar salterns. Appl Environ Microbiol 66:3052–3057

Antón J, Oren A, Benlloch S, Rodríguez-Valera F, Amann R, Rosselló-Móra R (2002) *Salinibacter ruber* gen. nov., sp. nov., a novel, extremely halophilic member of the Bacteria from saltern crystallizer ponds. Int J Syst Evol Microbiol 52:485–491

Antón J, Peña A, Santos F, Martinez-Garcia M, Schmitt-Kopplin P, Rosselló-Móra R (2008) Distribution, abundance and diversity of the extremely halophilic bacterium *Salinibacter ruber*. Saline Syst 4:15

Barker M, Rayens W (2003) Partial least squares for discrimination. J Chemom 17:166–173

Bylesjö M, Rantalainen M, Cloarec O, Nicholson J, Holmes E, Trygg J (2006) OPLS discriminant analysis: combining the strengths of PLS-DA and SIMCA classification. J Chemom 20:341–351

Coucheney E, Daniell TJ, Chenu C, Nunan N (2008) Gas chromatographic metabolic profiling: a sensitive tool for functional microbial ecology. J Microbiol Methods 75:491–500

Coutard F, Crassous P, Droguet M, Gobin E, Colwell RR, Pommepuy M, Hervio-Heath D (2007) Recovery in culture of viable but nonculturable *Vibrio parahaemolyticus*: regrowth or resuscitation? ISME J 1:111–120

Denich TJ, Beaudette LA, Lee H, Trevors JT (2003) Effect of selected environmental and physico-chemical factors on bacterial cytoplasmic membranes. J Microbiol Methods 52:149–182

DiRusso CC, Black PN, Weimar JD (1999) Molecular inroads into the regulation and metabolism of fatty acids, lessons from bacteria. Prog Lipid Res 38:129–197

Ede SM, Hafner LM, Fredericks PM (2004) Structural changes in the cells of some bacteria during population growth: a Fourier transform infrared-attenuated total reflectance study. Appl Spectrosc 58:317–322

Fekete A, Kuttler C, Rothballer M, Hense BA, Fischer D, Buddrus-Schiemann K, Lucio M, Müller J, Schmitt-Kopplin P, Hartmann A (2010) Dynamic regulation of N-acyl-homoserine lactone production and degradation in *Pseudomonas putida* IsoF. FEMS Microbiol Ecol 72:22–34

García DE, Baidoo EE, Benke PI, Pingitore F, Tang YJ, Villa S, Keasling JD (2008) Separation and mass spectrometry in microbial metabolomics. Curr Opin Microbiol 11:233–239

Hertkorn N, Ruecker C, Meringer M, Gugisch R, Frommberger M, Perdue EM, Witt M, Schmitt-Kopplin P (2007) High-precision frequency measurements: indispensable tools at the core of the molecular-level analysis of complex systems. Anal Bioanal Chem 389:1311–1327

Höller C, Witthuhn D, Janzen-Blunck B (1998) Effect of low temperatures on growth, structure, and metabolism of *Campylobacter coli* SP10. Appl Environ Microbiol 64:581–587

Holmes E, Antti H (2002) Chemometric contributions to the evolution of metabonomics: mathematical solutions to characterising and interpreting complex biological NMR spectra. Analyst 127:1549–1557

Kanehisa M, Goto S (2000) KEGG: Kyoto encyclopedia of genes and genomes. Nucleic Acids Res 28:27–30

Lattanzio VM, Baronio M, Oren A, Russell NJ, Corcelli A (2009) Characterization of polar membrane lipids of the extremely halophilic bacterium *Salinibacter ruber* and possible role of cardiolipin. Biochim Biophys Acta 1791:25–31

Li X, Fekete A, Englmann M, Gotz C, Rothballer M, Frommberger M, Buddrus K, Fekete J, Cai C, Schroder P, Hartmann A, Chen G, Schmitt-Kopplin P (2006) Development and application of a method for the analysis of N-acylhomoserine lactones by solid-phase extraction and ultra high pressure liquid chromatography. J Chromatogr A 1134:186–193

Lucio M, Fekete A, Schmitt-Kopplin P (2010) High resolution tools offer to follow bacterial growth on a molecular level. In: Handbook of Molecular Microbial Ecology I Metagenomics and Complementary Approaches. Wiley-Blackwell ISBN: 978-0-470-64479-9

Mashego MR, Rumbold K, De Mey M, Vandamme E, Soetaert W, Heijnen JJ (2007) Microbial metabolomics: past, present and future methodologies. Biotechnol Lett 29:1–16

Mongodin EF, Nelson KE, Daugherty S, Deboy RT, Wister J, Khouri H, Weidman J, Walsh DA, Papke RT, Sánchez-Pérez G, Sharma AK, Nesbo CL, MacLeod D, Bapteste E, Doolittle WF, Charlebois RL, Legault B, Rodríguez-Valera F (2005) The genome of *Salinibacter ruber*: convergence and gene exchange among hyperhalophilic bacteria and archaea. Proc Natl Acad Sci USA 102:18147–18152

Nichols DS, Olley J, Garda H, Brenner RR, McMeekin TA (2000) Effect of temperature and salinity stress on growth and lipid composition of *Shewanella gelidimarina*. Appl Environ Microbiol 66:2422–2429

Peña A, Teeling H, Huerta-Cepas J, Santos F, Yarza P, Brito-Echeverría J, Lucio M, Schmitt-Kopplin P, Meseguer I, Schenowitz C, Dossat C, Barbe V, Dopazo J, Rosselló-Móra R, Schuler M, Glockner FO, Amann R, Gabaldon T, Antón J (2010) Fine-scale evolution: genomic, phenotypic and ecological differentiation in two coexisting *Salinibacter ruber* strains. ISME J 4:882–895

Rosselló-Móra R, Lucio M, Peña A, Brito-Echeverría J, López-López A, Valens-Vadell M, Frommberger M, Antón J, Schmitt-Kopplin P (2008) Metabolic evidence for biogeographic isolation of the extremophilic bacterium *Salinibacter ruber*. ISME J 2:242–253

Samuel BS, Hansen EE, Manchester JK, Coutinho PM, Henrissat B, Fulton R, Latreille P, Kim K, Wilson RK, Gordon JI (2007) Genomic and metabolic adaptations of *Methanobrevibacter smithii* to the human gut. Proc Natl Acad Sci USA 104:10643–10648

Schaub J, Reuss M (2008) In vivo dynamics of glycolysis in *Escherichia coli* shows need for growth-rate dependent metabolome analysis. Biotechnol Prog 24:1402–1407

Suhre K, Schmitt-Kopplin P (2008) MassTRIX: mass translator into pathways. Nucleic Acids Res 36:W481–W484

Trygg J, Wold S (2002a) Orthogonal projections to latent structures (O-PLS). J. Chemom 16:119–128

Trygg J, Wold S (2002b) O2-PLS, a two-block (X-Y) latent variable regression (LVR) method with an integral OSC filter. J. Chemom 17:53–64

Wu Z, Rodgers RP, Marshall AG (2004) Two- and three-dimensional van krevelen diagrams: a graphical analysis complementary to the Kendrick mass plot for sorting elemental compositions of complex organic mixtures based on ultrahigh-resolution broadband Fourier transform ion cyclotron resonance mass measurements. Anal Chem 76:2511–2516